CrossMark

Isotopes and hydrochemistry of Daihai Lake recharging sources, Northern China

Tao Wang[1] · Jiansheng Chen[1] · Yi Xu[1] · Lucheng Zhan[1] · Dewen Huang[1]

Abstract Daihai Lake has faced severe shrinkage in recent years due to over-exploitation. Stable isotopes (D and ^{18}O) and hydrochemistry are employed to investigate the source of lake water to better understand its recharge dynamics. Results show that, in additional to local rainfall, groundwater is also an important water supply to the lake and accounts for a greater proportion. The groundwater is not recharged by local rainfall, but originates from other sources with significantly depleted isotope values. Combined with springs and artesian wells in the basin, it is consistent with the recent discover of external groundwater recharging in Northern China.

Keywords Groundwater · Hydrogen and oxygen stable isotopes · Hydrochemistry · Soil profile · Daihai Lake basin

Introduction

Daihai Lake basin is located in an arid/semi-arid area of Northern China, where annual evaporation far exceeds precipitation. The area suffers from surface water shortages, which has resulted in severe desertification, with regional deserts including the Bayinwenduer, Kubuqi, Maowusu, and Wulanbuhe [1]. However, the area also has a number of lakes, including Daihai, Wuliansuhai, Huanqihai, and Daliluoer. Daihai and Huangqihai lakes are

tectonic basins 64 km apart, with similar geology, hydrogeology, formation and evolution processes [2–4]. Both lakes contain rich natural resources and have played a key role both in the development of local economy and in domestic water security. Owing to over-exploitation of groundwater, Huangqihai Lake has decreased in area and water equality since the 1980s, and has now dried up [3]. Although there has also been a sharp drop in the area of Daihai Lake in recent years, most studies have focused on lake sediment [4–11], with limited investigation of water cycle. Feng [12] used the water balance model to show that Daihai Lake was recharged by surface and subsurface runoff from local precipitation, while Chen [1] used the isotope signature to confirm that the lake is recharged by both groundwater and rainfall, but the former is not itself recharged by local precipitation.

Stable isotopic indicators have been widely used as tracers of interactions between different sources of water (e.g., precipitation, surface water, soil water, and groundwater), as well as their recharge and discharge in the hydrological cycle, especially in semi-arid and arid regions [13, 14]. Greater insight into the origin and behavior of major ions in different water sources would enhance our understanding of geochemical evolution during recharge and discharge [15, 16]. For example, using stable isotope and hydrochemistry in Subei Lake basin, Liu [17] concluded that the lake water, which was undergoing intense evaporation, was recharged from overland flow and groundwater, and that the groundwater was of modern local meteoric origin rather than recharge from precipitation in paleoclimate conditions.

Stable isotope and geochemistry profiles of the unsaturated zone have also been employed to investigate the recharge and discharge of soil water [18, 19]. Using δD, δ^{18}O, and chloride profiles, Chen [20] showed that soil

✉ Jiansheng Chen
jschen@hhu.edu.cn

[1] Geotechnical Research Institute, College of Civil and Transportation Engineering, Hohai University, Nanjing 210098, China
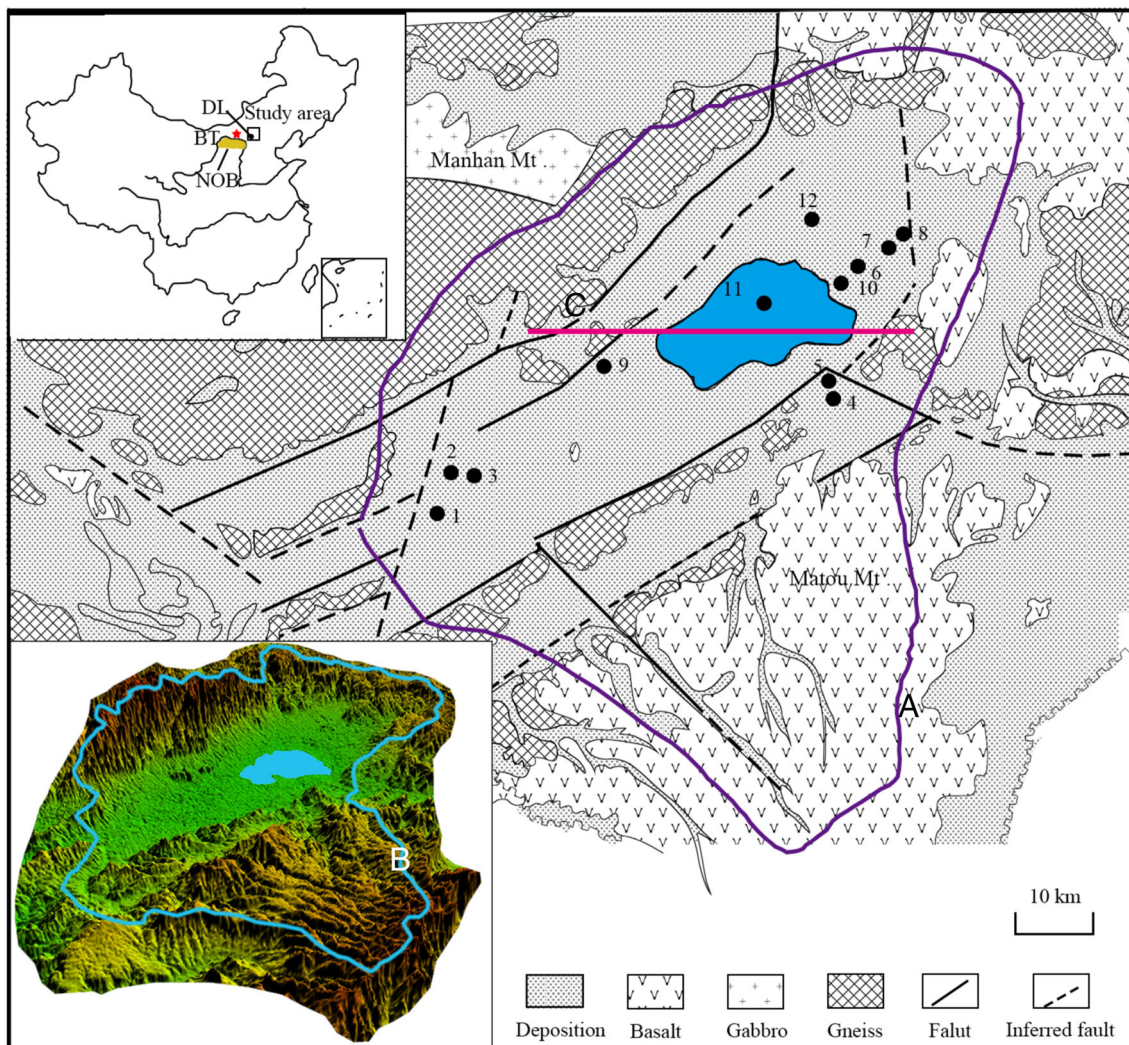
Fig. 1 Geologic map of the Daihai Lake basin study area [4–6]. *Lines A* and *B* mask the border of Daihai Lake basin. *Numbers* refer to the location of boreholes in Fig. 2, and *line C* is the cross-section in Fig. 2b. *NOB* Northern Ordos Basin, *DL* Daihai Lake, *BT* Baotou, *Mt.* Mountain

water experiences two stages of evaporation. During the first stage, the stable isotopes in unsaturated soil change exponentially with depth, similar to those in saturated soil profiles. In the second stage, the soil surface begins to dry and the evaporation rate falls to a quasisteady state. Huang [21] used relatively deep soil profiles and multiple tracers (chloride mass balance, stable isotopes, tritium, and water chemistry) to investigate groundwater recharge rates, ages, and mechanisms in one area of the Loess Plateau in China.

This study combines hydrogen and oxygen stable isotopes with hydrochemistry, and aims to investigate the relationship of water recharge and discharge in Daihai Lake basin, to better understand recharge dynamics for improved future management and exploitation. To compare Daihai Lake results with Huangqihai Lake, the study area was extended to include the northern Huangqihai Lake basin.

Study area

Geological conditions in the study area

Lake Daihai basin (112°33′31″–112°46′40″E, 40°29′27″–40°37′06″N, 1220 meters above sea level) is an enclosed inland rift basin formed at the start of the Quaternary in northern central China, which is bordered to the north by the Manhan Mountain, and to the south by the Matou Mountain (Fig. 1). Two main fault groups are distributed along NE/NNE–SW/SE direction [4–6]. They are formed during the Yanshan movement, and directly control the topographic feature in this area. The Daihai Lake basin is progressively filled by diluvial plain, alluvial plain, and lacustrine deposits, from the base of the mountains to the lake. It is covered by a layer of loess during the late Quaternary. The basement of the basin is pre-Sinian
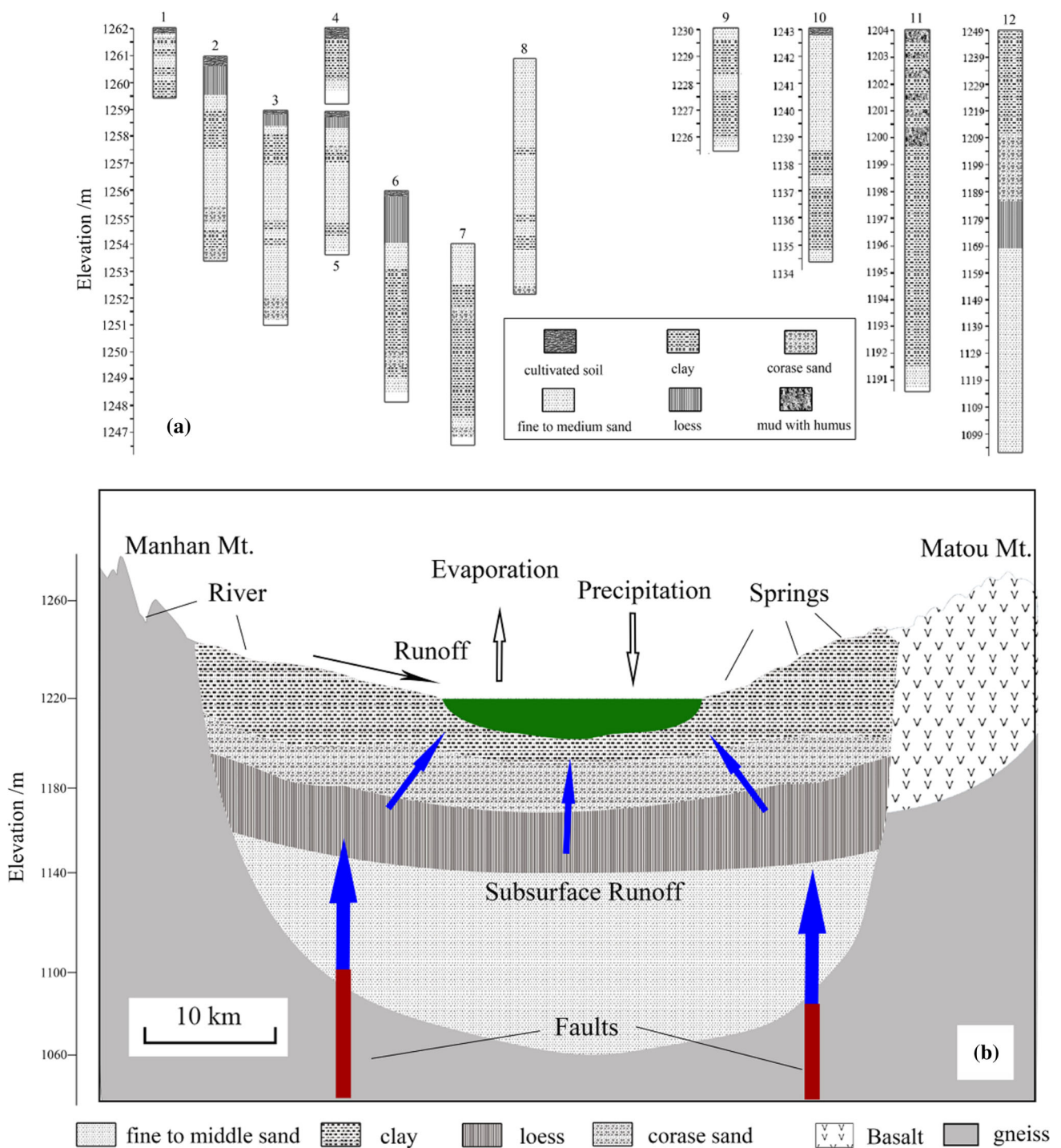
Fig. 2 a Daihai Lake basin borehole geology. No. 1 to 8 share the same elevation. Borehole locations are as in Fig. 1; **b** Inferred cross-section (*line C* in Fig. 1) beneath Daihai Lake basin

granitic gneiss, with basalts emplaced from the late Tertiary to Quaternary in the east and south, and a small area of Mesozoic volcanic in the northwest.

Several borehole sections are available for Daihai Lake basin, as shown in Fig. 2 [7]. Borehole DH-99B (11) is drilled in the depositional center of the lake with a depth of 12.87 m and Maituhu (12) has the largest depth of 156 m. Borehole DH-99B shows that the depositions downward over the lake water area are mud with humus, clay and fine to medium sand. While, outside the water area, the other boreholes overall shows the downward depositions of cultivated soil, clay, loess, and fine to medium.
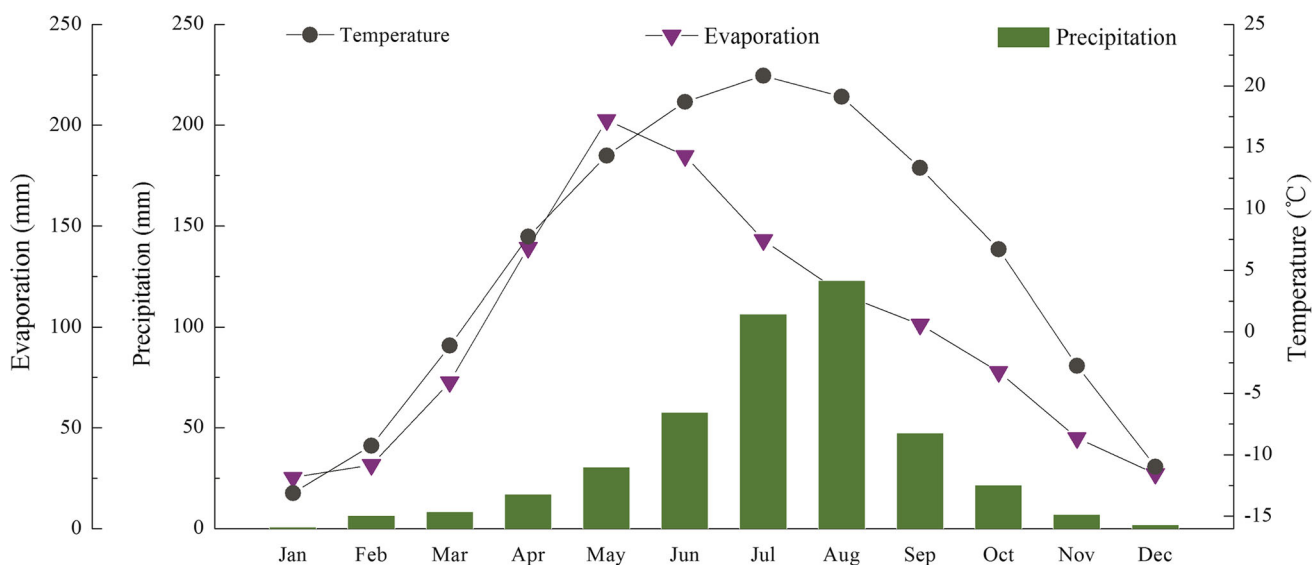
Fig. 3 Monthly variations in temperature, evaporation, and precipitation in the study area
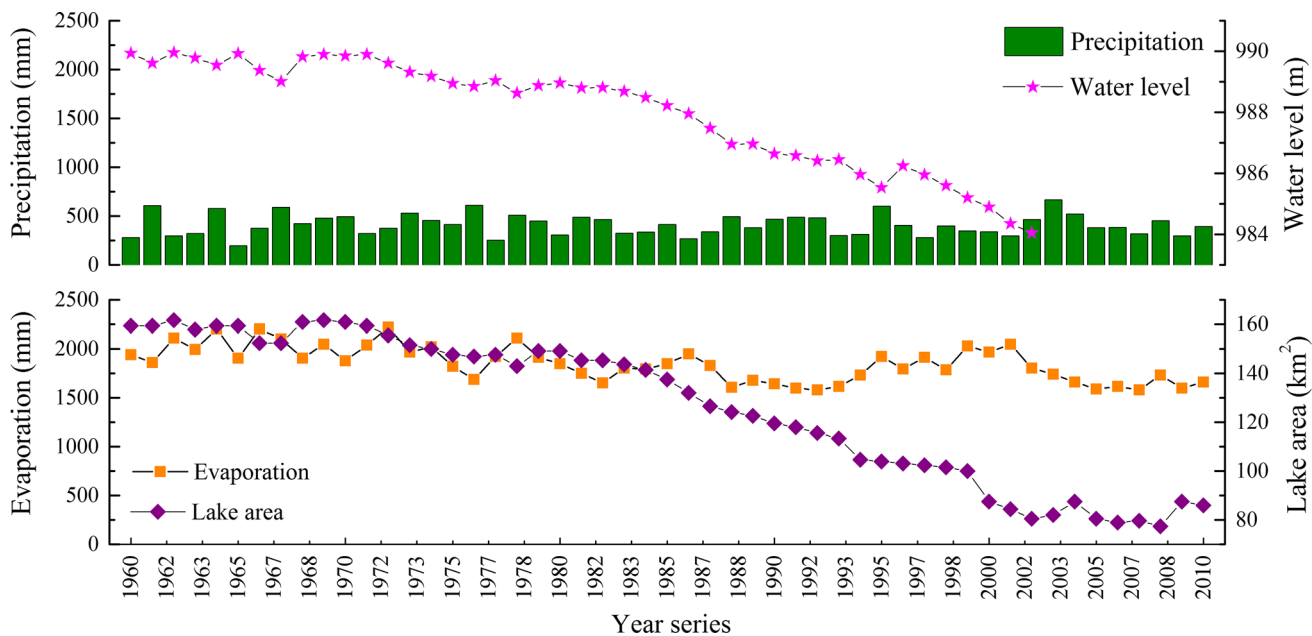

Fig. 4 Interannual variation of evaporation, precipitation, water level, and lake area for Daihai Lake [23]. Note that the water level is relative to the assumed elevation of observation station

Meteorological conditions in the study area

The lake basin is located in the monsoonal/arid transition zone [8–10]. In winter, the climate is controlled by a cold continental high-pressure system, dominated by the Siberian–Mongolian High. In summer, warm and moist air originating from low latitudes (i.e., the ocean) can reach the lake and increase precipitation. The mean monthly temperature in the lake drainage basin is −13 to −15 °C in January, and it peaks at 17–20.5 °C in July. Precipitation starts to increase in February, and peaks in August; rainfall between June and September, brought by summer monsoon moisture represents ∼66% of the annual 350–450 mm of precipitation. Mean annual evaporation is 1938 mm, mainly occurring from April to July. Evaporation levels are lowest during the sub-freezing winter, and then peak in May before declining during the summer owing to an increase in both rainfall and humidity and a decrease in wind (Fig. 3). Vegetation is influenced by topography; from the mountains in the northwest to the Daihai basin, vegetation changes from arid forest to shrub grass land then semi-arid grassland [9, 22].
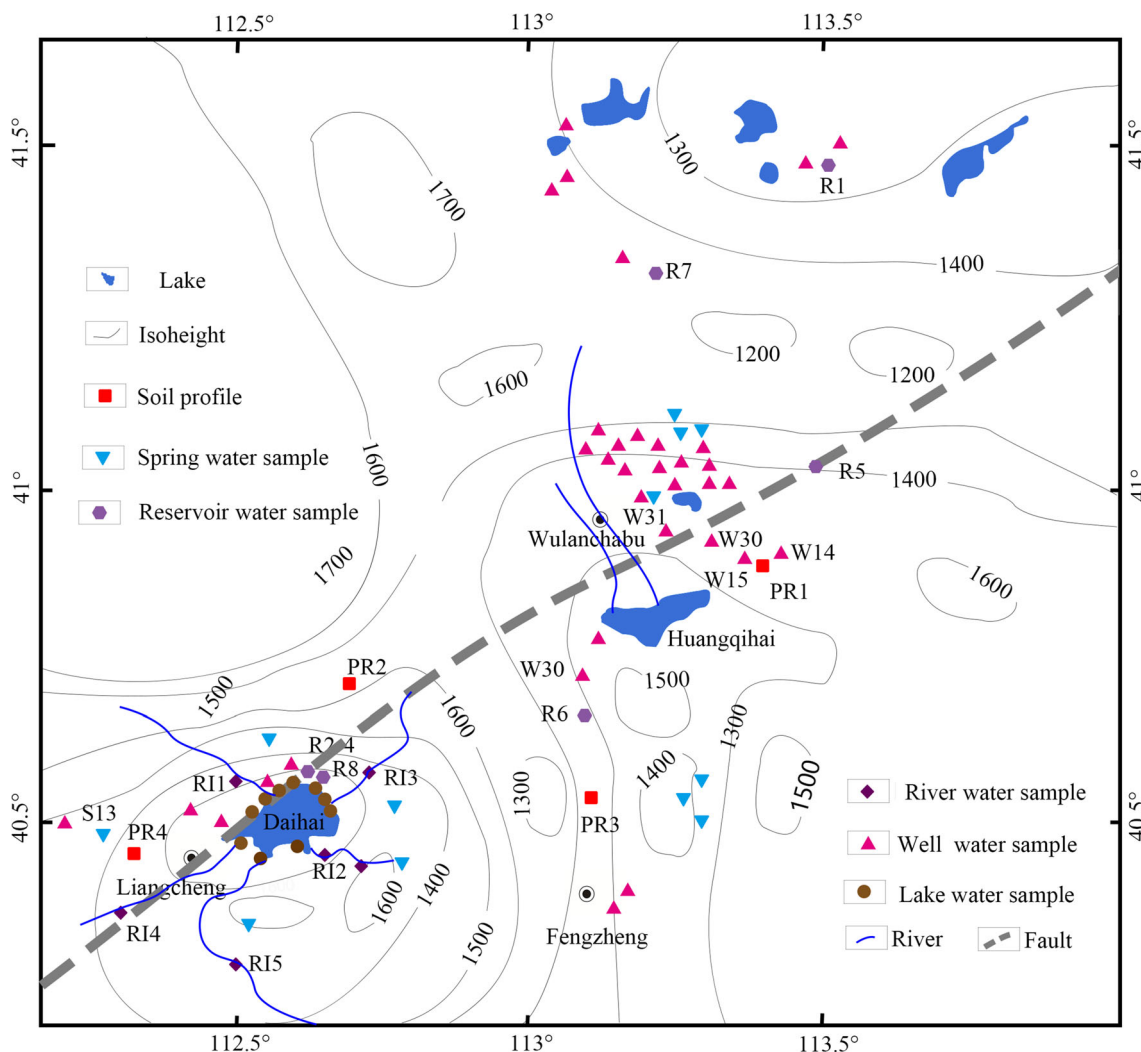
Fig. 5 Map of the study area showing sampling sites

Daihai Lake extends 20 km along a NW–SE axis, and has a maximum width of 14 km perpendicular to that axis [7, 8]. Geomorphologically, at least two terrace levels, 15–20 and 30–40 m above the present lake surface, can be identified around the southwest and northeast parts of the lake basin. The total area of the lake is 160 km^2, and it has a maximum water depth of 16 m and a drainage area of 2289 km^2. Over 20 rivers run into Daihai Lake, of which the main rivers are Gongba River, Wuhao River, Tiancheng River, and Muhua River, which supply the lake all year round. They are mostly located in the eastern and southern parts of the basin, with a main orientation of NW–SE controlled by faults. Other rivers, which originate from the northern mountainous area, are seasonal. Since there is no outflow from the lake, water is only lost through evaporation [8]. The water level in Daihai Lake decreased from ∼990 m in 1960 to ∼984 m in 2002, with a sharp decline since 1980, despite little variation in evaporation and precipitation. The continued shrinkage in lake area is

due to high groundwater consumption (Fig. 4); hence, there is an urgent need to investigate the basin water cycle for improved water management.

Materials and methods

Water sampling

Several field visits and sampling campaigns were conducted during 2009–2012 in the Daihai and Huangqihai Lake basins and nearby, and a total number of 71 water samples were collected (Fig. 5; Table 1). All water samples were collected in 550-ml plastic bottles, which had been washed twice with sample water. Then, the bottle was capped quickly and sealed tightly with tape retaining, retaining as few bubbles as possible. All samples were stored in a freezer to avoid isotope fractionation before measurement. The total dissolved solids (TDS) of water

Table 1 Water samples information and measured results of isotopes and water chemistry

Date	No.	Longitude (Time degree)	Latitude (Time degree)	Elevation (m)	δD (‰)	$\delta^{18}O$ (‰)	TDS (mg/L)	Ca^{2+} (mg/L)	Ma^{2+} (mg/L)	Na^+ & K^+ (mg/L)	CO_3^{2-} & HCO_3^- (mg/L)	SO_4^{2-} (mg/L)	Cl^- (mg/L)
May-09	S1	113.2694°	41.0403°	1358	−70.10	−8.70	291	68.50	24.40	28.10	328.30	23.10	29.00
	S2	113.3465°	41.1157°	1589	−73.10	−9.20	114	49.60	14.00	11.70	205.60	24.00	10.10
	S3	113.3465°	41.1461°	1654	−71.60	−8.90	220	84.20	40.20	52.60	542.80	21.50	17.80
	S4	113.3465°	40.5767°	1415	−71.00	−9.60	256	62.00	16.10	33.90	57.38	41.00	42.10
	S5	113.3465°	40.5615°	1410	−80.50	−11.10	337	71.88	17.77	51.46	385.80	17.00	22.50
	S6	113.3465°	40.5929°	1414	−74.00	−10.20	268	45.20	12.43	43.30	252.70	21.47	20.90
	W1	113.2503°	41.0670°	1368	−71.30	−8.60	146	72.30	19.90	10.80	298.00	24.50	12.30
	W2	113.2481°	41.0680°	1367	−72.10	−8.80	112	51.20	18.00	11.40	245.10	14.30	8.50
	W3	113.2683°	41.0421°	1358	−70.20	−8.60	270	91.80	29.50	20.90	335.90	31.20	63.90
	W4	113.3039°	41.0879°	1432	−72.40	−8.40	212	81.90	24.90	20.00	330.10	36.80	30.60
	W5	113.3557°	41.0956°	1449	−75.10	−9.20	197	81.20	26.20	35.50	411.60	31.40	13.70
	W6	113.3671°	41.0784°	1422	−63.90	−7.80	192	45.00	20.30	99.80	367.20	44.30	47.50
	W7	113.3763°	41.0542°	1387	−64.70	−7.40	550	133.50	66.50	88.60	622.50	129.20	112.60
	W8	113.3674°	41.0418°	1370	−74.90	−9.30	215	38.60	16.20	99.80	383.50	33.00	22.90
	W9	113.2843°	41.1156°	1452	−76.00	−11.30	616	143.10	56.50	124.50	684.20	68.90	164.20
	W10	113.1848°	41.1077°	1383	−68.40	−8.90	391	74.40	30.60	149.60	597.80	68.30	55.10
	W11	112.5682°	40.5629°	1240	−78.50	−10.80	229	78.86	11.12	32.96	295.40	27.60	31.40
	W12	113.2547°	41.0957°	1399	−70.40	−9.10	236	65.30	35.00	46.90	391.00	42.70	32.70
	W13	113.1835°	41.1121°	1386	−69.10	−8.80	218	50.50	31.10	59.10	365.10	35.10	34.40
	W14	113.4606°	40.9469°	1444	−68.50	−8.90	150	44.70	15.20	46.70	286.40	11.00	21.60
	W15	113.4869°	40.9467°	1449	−73.80	−9.10	177	61.90	27.70	32.50	358.80	24.20	15.30
	W16	112.5682°	40.5629°	1240	−78.50	−10.80	229	78.86	11.12	32.96	295.40	27.60	31.40
	W17	113.2030°	40.8211°	1274	−70.60	−8.60	197	57.60	28.50	45.10	354.90	32.60	25.50
	W18	113.1703°	40.7680°	1363	−69.10	−8.50	556	154.90	71.20	30.00	666.60	68.90	93.00
	W19	113.2715°	40.3495°	1169	−67.70	−7.90	330	85.50	36.20	49.80	374.10	54.80	77.50
	W20	113.2684°	41.3835°	1499	−73.60	−9.00	492	42.20	61.10	104.10	340.60	97.70	145.80
	W21	113.1349°	41.5148°	1465	−70.50	−8.80	195	20.50	17.80	64.30	179.00	33.70	59.20
	W22	113.1349°	41.5148°	1465	−79.40	−10.20	200	50.60	19.30	49.70	265.20	37.20	41.80
	W23	113.5772°	41.5321°	1418	−80.20	−9.90	495	68.40	42.80	126.70	398.80	142.40	106.20
	W24	113.1728°	41.5900°	1469	−76.60	−9.50	213	71.30	22.50	26.70	289.50	44.80	32.70
	W25	112.6446°	40.6236°	1268	−76.20	−10.50	135	43.30	10.70	40.50	239.30	22.00	15.50
	W26	112.7485°	40.6149°	1231	−76.60	−10.60	273	56.05	20.14	26.68	293.10	15.78	18.00
	W27	112.2255°	40.5304°	1730	−76.70	−10.90	241	54.98	14.24	30.45	271.00	19.51	14.60
	R1	113.5709°	41.5311°	1418	−39.00	−1.40	1526	36.80	74.60	513.20	493.90	305.60	564.70
	R2	112.7484°	40.6143°	1231	−42.40	−3.00	392	47.89	30.70	52.60	348.20	9.82	47.10
	R3	112.7468°	40.615°	1230	−56.70	−5.60	311	37.09	33.09	43.58	330.40	8.78	32.20

Table 1 continued

Date	No.	Longitude Time degree	Latitude Time degree	Elevation (m)	δD (‰)	δ¹⁸O (‰)	TDS (mg/L)	Ca²⁺ (mg/L)	Ma²⁺ (mg/L)	Na⁺ & K⁺ (mg/L)	CO₃²⁻ & HCO₃⁻ (mg/L)	SO₄²⁻ (mg/L)	Cl⁻ (mg/L)
	R4	112.7460°	40.6158°	1230	−46.70	−3.90	365	35.94	29.12	53.18	291.30	16.07	50.60
	L1	112.6431°	40.5929°	1225	−6.20	2.00	6050	35.89	185.40	2096.00	424.70	168.40	3476.00
	L2	112.6460°	40.5945°	1224	−6.60	2.20	6070	33.79	152.40	2154.00	637.70	164.80	3342.00
Jul-11	S7	113.3460°	41.1211°	1635	−78.60	−9.70	192	44.70	14.00	9.80	194.00	20.70	7.70
	W28	113.3370°	41.0620°	1403	−67.90	−8.30	223	92.10	24.90	23.90	373.30	34.70	31.10
	W29	113.2003°	41.0944°	1374	−72.50	−8.80	283	98.60	29.70	27.00	367.80	31.50	67.20
	W30	113.3845°	40.9675°	1322	−67.50	−8.30	170	43.80	33.30	35.80	339.00	26.80	14.40
	W31	113.3067°	40.9807°	1311	−67.70	−7.90	176	44.30	53.50	17.00	375.40	31.30	21.50
	W32	113.2036°	40.4055°	1196	−67.80	−8.40	220	21.20	13.60	117.30	356.40	29.90	29.40
	W33	113.6094°	41.5686°	1436	−86.10	−11.00	523	40.10	35.10	121.40	110.40	100.90	223.50
	W34	112.6380°	40.6258°	1281	−91.70	−12.10	853	55.90	12.70	191.40	699.70	123.80	123.80
	R5	113.5714°	41.0668°	1394	−39.50	−1.90	215	12.80	33.60	66.10	234.50	52.00	49.20
	R6	113.1626°	40.7180°	1419	−4.50	3.70	3344	2.70	110.30	1284.00	666.40	67.70	1875.00
	R7	113.2805°	41.3744°	1502	−44.00	−2.60	898	25.50	39.30	110.90	413.80	46.20	57.70
	R8	112.7497°	40.6138°	1231	−44.40	−3.40	346	33.41	29.55	63.23	266.40	45.91	55.30
	L3	112.6406°	40.5903°	1225	−5.30	2.40	6010	32.73	171.80	2214.00	712.50	155.30	3454.00
	L4	112.6709°	40.5930°	1220	−6.90	1.90	5970	31.49	178.20	2244.00	1324.00	176.70	3146.00
	L5	112.7383°	40.5961°	1219	1.20	4.10	6099	26.83	196.80	2231.00	1169.00	194.20	3250.00
	RI1	112.5155°	40.5632°	1228	−40.00	−2.40	429	56.48	40.73	62.63	454.60	38.02	24.74
	RI2	112.7576°	40.4999°	1320	−41.50	−4.60	419	63.72	12.84	22.17	257.40	24.00	17.79
	RI3	112.8057°	40.6205°	1421	−44.50	−4.60	619	73.62	22.94	32.47	354.30	32.00	18.79
May-12	S8	112.6361°	40.6831°	1279	−76.60	−8.70	313	10.04	21.78	34.30	137.00	33.82	30.46
	S9	112.8404°	40.5855°	1340	−79.50	−9.90	431	48.40	21.46	36.98	307.20	20.16	12.78
	S10	112.8405°	40.4967°	1352	−84.50	−10.50	373	40.00	13.34	34.75	230.50	21.98	13.74
	S11	112.6918°	40.4321°	1398	−80.70	−9.40	457	55.24	18.34	33.97	265.10	39.94	20.91
	S12	112.5344°	40.4188°	1385	−71.90	−9.70	422	62.72	20.74	26.06	309.90	18.14	19.10
	S13	112.3671°	40.5139°	1266	−85.30	−11.60	295	44.52	10.15	12.31	179.30	20.74	8.38
	L6	112.6166°	40.5733°	1221	−6.60	3.90	6015	34.64	132.90	2230.00	1149.00	139.40	3125.00
	L7	112.6164°	40.5637°	1220	−7.80	3.20	6165	34.40	131.40	2321.00	1091.00	133.70	3299.00
	L8	112.7479°	40.5813°	1221	−1.70	3.20	6229	33.92	129.20	2185.00	711.10	141.30	3297.00
	L9	112.7341°	40.5994°	1223	0.80	3.90	6105	34.32	131.20	2305.00	1158.00	147.90	3224.00
	L10	112.7281°	40.5548°	1223	−4.20	2.50	6260	28.68	240.00	2256.00	1116.00	141.30	3489.00
	L11	112.6438°	40.5346°	1224	−3.80	2.50	6580	20.16	252.00	2382.00	1180.00	155.90	3656.00
	RI4	112.3941°	40.3976°	1398	−37.00	−1.60	424	58.28	18.82	25.32	271.80	31.30	16.90
	RI5	112.5155°	40.4073°	1423	−38.50	−3.70	565	61.80	18.00	21.44	285.30	20.45	14.87

Table 1 continued

Date	No.	Longitude	Latitude	Elevation	δD	δ¹⁸O	TDS	Ca²⁺	Ma²⁺	Na⁺ & K⁺	CO₃²⁻ & HCO₃⁻	SO₄²⁻	Cl⁻
		Time degree	Time degree	(m)	(‰)	(‰)	(mg/L)	(mg/L)	(mg/L)	(mg/L)	(mg/L)	(mg/L)	(mg/L)
S average					-76.72 ± 1.44	-9.78 ± 0.25	305.31 ± 27.61	52.85 ± 5.06	18.82 ± 2.13	31.48 ± 3.85	261.20 ± 33.6	24.89 ± 2.22	19.65 ± 2.73
W average					-73.12 ± 1.01	-9.26 ± 0.20	291.62 ± 28.89	67.48 ± 5.31	29.03 ± 2.77	60.00 ± 2.77	369.47 ± 23.36	47.01 ± 5.82	54.08 ± 8.63
R average					-39.65 ± 5.39	-2.26 ± 0.97	924.63 ± 378.61	29.02 ± 5.20	47.53 ± 10.43	273.35 ± 154.83	380.61 ± 50.28	69.01 ± 34.65	341.48 ± 228.20
L average					-4.28 ± 0.94	2.89 ± 0.24	6141.18 ± 51.69	31.53 ± 1.40	172.85 ± 13.11	2238.00 ± 23.97	970.27 ± 88.08	156.26 ± 5.55	3341.64 ± 48.85
RI average					-40.30 ± 1.29	-3.38 ± 0.60	491.20 ± 42.06	62.78 ± 2.99	22.67 ± 4.79	32.81 ± 7.71	324.68 ± 36.79	29.15 ± 3.11	18.62 ± 1.66

Average values are shown by 'mean value ± standard error'

S spring water, W well water, R reservoir water, L lake water, RI river water

samples were measured with a desk TDS/NaCl tester (Model: HI2300). For measurements of $\delta^{18}O$, δD, and ion concentrations, water samples were filtered using a medium-speed quantitative filter paper. Then, the $\delta^{18}O$ and δD were measured using a gas-source mass-spectrometer (Model: MAT 253) by the $CO_2–H_2O$ equilibration method and by reduction to H_2 over hot metallic zinc, respectively, at the State Key Laboratory of Hydrology-Water Resources and Hydraulic Engineering, Hohai University [24, 25]. Isotopic data are reported in the standard delta notation, in parts per thousand relative to Vienna Standard Mean Ocean Water. The $\delta^{18}O$ and δD values have an overall precision of 0.2‰ and 2‰, respectively. The measurement of positive ions (Ca^{2+}, Mg^{2+}, Na^+, and K^+) was conducted by an iCAP 6000 Series ICP-OES Spectrometer; the measurement of negative ions (SO_4^{2-} and Cl^-) was conducted by a Dionex ICS-2000 ion chromatography system. The precision of the cation and anion measurement is >95%. Anions (CO_3^{2-} and HCO_3^-) were analyzed by phenothalin and methyl-orange double indicator titration.

Soil profiles

Four soil profiles (PR) were sampled at intervals of 30 or 50 cm up to a maximum depth of 800 cm (Fig. 5; Table 2). Soil samples of ∼500 g were collected with a bucket auger and embedded in an aluminum specimen box that was sealed with tape. The moisture content by weight was determined by sample weight loss during oven drying at 105 °C for 24 h, with an analytical precision of $\geq 1\%$ [1]. Soil water for isotope measurements of D and ^{18}O was extracted using vacuum distillation following the procedure of Shurbaji et al. [26]. For measurement of ion concentrations in soil water, soil samples were oven dried for 48 h, and then 100 g of the dried soil was mixed with 100 ml of deionized water. The mixture was allowed to equilibrate for 48 h, during which it was periodically stirred. After equilibration, the leachate was filtered using a medium-speed quantitative filter paper. The pretreatment and measurement of $\delta^{18}O$, δD, TDS, and the main cation and anions was as described above. Ion concentrations were calculated based on the mass conservation of each ion using the relationship (with Cl^- used as an example): $Cl_{sw} = Cl_{le}/\theta$, where cl_{sw} is the original chloride concentration of soil water, cl_{le} is the chloride concentration of the leachate, and θ is the moisture content by weight.

Results

Water isotopes analysis

The relationships between spring, well, lake, river, reservoir, soil, and rainfall water are shown in Fig. 6. Spring water

Table 2 Soil profile information

No.	Date	Elevation (m)	Longitude Time degree	Latitude Time degree	No.	Date	Elevation (m)	Longitude Time degree	Latitude Time degree
PR1	29-5-2009	1442	113°28.025′	40°55.971′	PR3	30-5-2009	1356	113°10.415′	40°35.458′
PR2	27-5-2009	1519	112°46.736′	40°45.547′	PR4	16-7-2011	1334	112°24.674′	40°30.353′

PR means soil profile

Fig. 6 Relationship between D and ^{18}O for different water sources. The area of each precipitation point is related to the monthly average rainfall. GMWL is the global meteoric water line, and EL1 and EL2 are evaporation lines (see text for details)
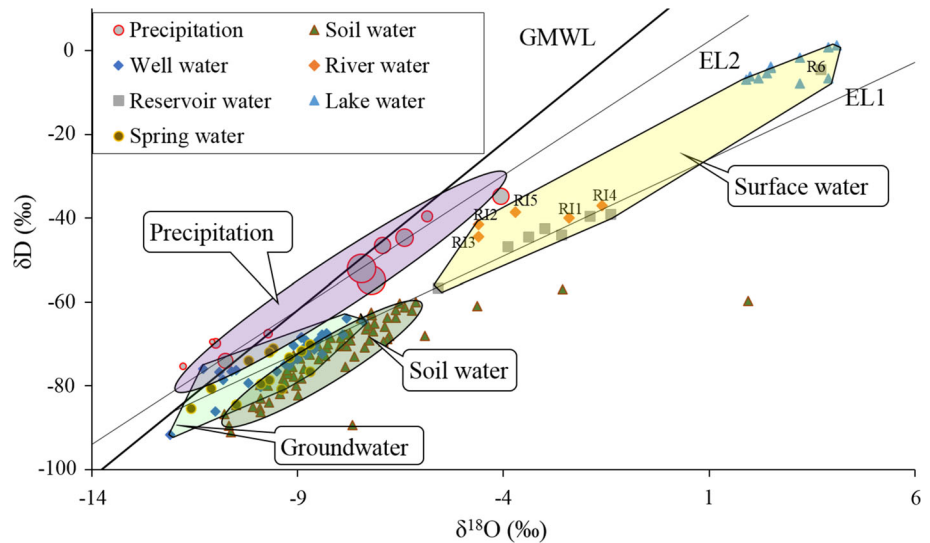
from both Daihai and Huangqihai lakes is closely clustered, as is well and soil water. As would be expected, spring and well water have similar isotope compositions, with mean values of −76.72 ± 1.44‰ and −73.12 ± 1.01‰ for δD, and −9.78 ± 0.25‰ and −9.26 ± 0.20‰ for δ^{18}O. They are designated as groundwater, which ranges from −91.7‰ to −63.9‰ for δD and from −12.1‰ to −7.4‰ for δ^{18}O. Mean isotope values of groundwater are −74.12‰ for δD and −9.41‰ for δ^{18}O. Lake, river, and reservoir water together comprise surface water, for which measured δD and δ^{18}O values range widely from −56.7‰ to 1.2‰ (with a mean value of −23.57‰) and from −5.6‰ to 4.1‰ (mean value of 0.13‰), respectively (Table 1). Distinct isotope compositions have the following order: lake water (mean δD and δ^{18}O values of −4.28 ± 0.94‰ and 2.89 ± 0.24‰) > reservoir water (mean δD and δ^{18}O values of −39.65 ± 5.39‰ and −2.26 ± 0.97‰) > river water (mean δD and δ^{18}O values of −40.3 ± 1.29‰ and −3.38 ± 0.60‰). Most soil water points cluster near to those for groundwater. The isotopic compositions of precipitation, groundwater, surface water, and soil water show distinct distributions. The enrichment of isotope values in surface water indicates significant evaporation. It should be noted that a few soil water points deviate from the main

group, showing rich isotope contents, which is attributed to intense evaporation.

Due to a lack of rainfall during the study period, it was not possible to collect rainfall samples. The Baotou station, from the Global Network of Isotopes in Precipitation (GNIP) [27, 28] was selected as a surrogate on the basis of its close proximity to the study area and relatively flat intervening terrain (Fig. 1). Precipitation, which undergoes little evaporation, should generally fall along the global meteoric water line (GMWL) [29–31]. Conversely, water types that undergo intense evaporation should display systematic enrichment in both δD and δ^{18}O, and lie along evaporation lines with slopes <8 (usually 4–6), deviating from the GMWL [31, 32]. The evaporation line for local precipitation, referred to hereafter as EL2, is fitted as δD = 6.42δ^{18}D − 4.03 (R^2 = 0.97), based on the monthly values of D and ^{18}O from Baotou station (Fig. 6). It is similar to the evaporation line for local precipitation (δD = 7.00δ^{18}O − 3.02) obtained using precipitation samples taken from the North Ordos basin in 2010–2011 [33], which is located close to the southwest of Daihai Lake (Fig. 1). EL2 lies below the GMWL, with some deviations, due to the strong evaporation in this semi-arid area [34, 35].

Table 3 Isotope and water chemistry in soil water

No.	Depth (cm)	δD (‰)	δ^{18}O (‰)	WC (%)	TDS (mg/L)	Cl$^-$ (mg/L)	SO$_4^{2-}$ (mg/L)	Na$^+$ (mg/L)	K$^+$ (mg/L)	Ma^{2+} (mg/L)	Ca^{2+} (mg/L)	CO$_3^{2-}$ & HCO$_3^-$ (mg/L)
PR1	0	−56.90	−2.56	3.72	7670	275.01	768.74	291.70	111.82	275.11	2388.88	4089.60
	30	−82.30	−8.99	3.99	8085	324.61	1926.46	308.59	70.52	264.39	2458.00	3380.43
	60	−85.30	−9.92	4.50	6590	166.57	2000.87	352.39	38.93	251.78	1752.49	2394.99
	90	−86.30	−9.90	5.07	4902	275.97	1095.44	288.65	26.80	204.57	1303.48	1977.80
	120	−77.80	−9.10	7.48	3697	115.63	904.13	245.56	20.28	162.63	983.61	1580.61
	150	−91.00	−10.62	5.58	4721	184.36	1044.85	449.63	28.03	212.81	1178.80	2133.87
	180	−89.60	−10.67	6.92	3419	132.75	519.86	406.31	25.66	157.83	773.72	1695.05
	210	−63.80	−6.61	9.92	2675	63.03	280.36	343.73	16.31	141.41	597.70	1506.87
	240	−63.90	−7.46	11.86	2554	55.33	311.23	345.18	15.24	146.69	554.73	1442.86
	270	−61.90	−6.61	13.17	2513	81.04	400.56	299.04	15.93	155.80	583.40	1370.22
	300	−66.50	−7.34	12.35	2266	45.88	210.58	316.80	14.84	141.53	468.58	1332.50
	330	−75.90	−8.84	10.05	2651	54.90	241.41	344.49	16.45	182.78	540.41	1557.50
	360	−85.00	−10.09	11.80	2019	47.42	216.80	259.07	15.17	127.87	388.57	1094.19
	390	−82.00	−9.42	12.52	1927	46.56	207.90	226.00	14.21	125.58	393.41	1057.58
	420	−86.80	−10.78	10.09	2134	59.88	182.59	228.65	15.94	145.13	450.35	1203.55
	450	−73.70	−8.48	11.81	1916	42.97	139.98	187.00	18.28	141.21	391.00	1091.22
	480	−78.30	−9.34	13.83	1658	52.42	155.68	147.47	16.49	114.20	360.88	904.77
	510	−70.60	−7.96	12.58	2109	57.81	167.49	168.10	26.05	141.86	481.23	1181.12
	540	−63.10	−7.19	11.61	2330	44.67	261.33	167.91	23.61	146.64	558.82	1261.13
	570	−67.40	−7.73	10.52	2194	71.44	211.52	191.27	26.44	160.87	574.57	1363.10
	600	−89.30	−7.66	10.88	2347	47.90	267.28	160.58	21.86	145.61	576.04	1267.17
	630	−70.90	−7.37	12.05	2291	57.60	254.07	156.25	24.42	144.36	567.46	1247.19
PR2	0	−68.10	−5.91	7.29	2955	104.29	433.86	191.26	24.50	93.36	795.64	1357.67
	30	−62.10	−6.22	12.37	1885	65.48	498.91	137.58	9.73	72.54	487.50	744.39
	60	−67.00	−7.16	11.75	1949	64.23	482.60	158.36	11.60	89.15	471.26	802.27
	90	−83.90	−9.70	10.49	1940	121.99	504.47	189.40	11.03	92.99	460.49	772.80
	120	−72.70	−9.10	12.73	1793	65.82	376.64	213.98	10.28	85.25	375.34	784.81
	150	−84.60	−10.49	11.29	1969	85.36	323.74	307.19	10.15	83.81	367.53	909.56
	180	−80.60	−9.34	13.28	1596	76.96	216.34	291.00	8.32	62.68	288.88	788.50
	210	−75.50	−9.12	12.75	1690	86.31	215.33	315.20	9.79	61.80	306.28	838.62
	240	−70.20	−7.93	11.44	1829	84.66	192.29	360.46	11.88	65.39	339.58	976.19
	270	−79.10	−9.32	12.04	1704	88.84	164.03	309.28	12.98	52.94	356.88	918.27
	300	−68.50	−8.20	9.87	1999	54.56	194.38	366.49	18.22	61.18	413.63	1115.79
	330	−71.00	−8.29	9.76	1992	73.99	195.59	344.87	16.47	68.86	435.05	1120.51
	360	−61.20	−6.39	11.42	1760	52.24	180.65	299.59	16.47	59.95	395.04	1005.00
PR3	0	−61.00	−4.64	5.35	5332	98.99	645.00	214.00	67.27	152.84	1752.44	2901.14
	30	−68.10	−6.77	5.77	6168	161.42	2236.83	353.45	46.32	238.81	1775.47	2258.59
	60	−68.80	−6.82	7.17	4212	87.01	1389.41	427.23	25.03	101.25	1191.36	1702.21
	90	−73.40	−8.94	5.61	4713	112.16	1086.46	956.00	25.37	71.01	998.35	2203.32
	120	−77.20	−9.24	4.20	6599	150.68	1656.08	1289.47	51.83	108.13	1347.83	2897.99
	150	−70.50	−8.50	4.98	5365	96.39	1399.44	1112.29	46.32	91.52	1042.89	2361.29
	180	−79.80	−9.91	8.37	4873	160.63	2412.31	892.51	25.46	112.14	919.76	1219.79
	210	−78.30	−8.90	8.96	4017	93.23	1673.20	887.94	24.13	79.44	700.18	1322.30
	240	−67.80	−7.85	9.45	4584	227.45	2135.21	702.97	30.49	132.92	937.76	1171.22
	270	−69.10	−7.26	8.95	4861	265.52	2014.76	658.66	31.45	157.76	1100.41	1468.18
	300	−70.60	−7.80	9.08	4316	313.56	1619.60	476.57	32.18	145.69	996.25	1247.58
	330	−65.60	−7.29	11.39	4134	382.50	782.22	401.20	31.65	153.95	1081.39	1770.89
	360	−60.30	−6.52	10.38	3893	317.04	1339.03	397.86	30.76	134.25	962.12	1236.28

Table 3 continued

No.	Depth (cm)	δD (‰)	$\delta^{18}O$ (‰)	WC (%)	TDS (mg/L)	Cl^- (mg/L)	SO_4^{2-} (mg/L)	Na^+ (mg/L)	K^+ (mg/L)	Ma^{2+} (mg/L)	Ca^{2+} (mg/L)	CO_3^{2-} & HCO_3^- (mg/L)
	390	−72.50	−8.71	10.68	3522	369.85	1033.92	312.34	30.76	117.91	869.46	1088.52
	420	−72.90	−8.33	11.96	2817	363.28	698.63	208.29	25.36	100.17	677.71	827.60
PR4	0	−59.70	1.95	3.04	4257	144.37	1139.02	115.61	22.55	76.48	1353.33	1580.93
	50	−75.40	−7.84	9.77	2273	74.08	379.64	51.20	2.86	16.20	348.33	337.58
	100	−73.00	−7.62	9.81	2146	30.16	364.77	50.45	2.39	15.24	278.28	274.16
	150	−83.00	−9.89	11.45	1874	20.76	176.86	42.19	2.75	14.91	214.58	292.95
	200	−79.90	−9.03	12.61	1778	15.99	141.54	33.40	1.57	13.61	169.42	234.79
	250	−79.90	−9.72	10.07	1834	23.32	142.07	55.89	1.00	19.90	191.00	306.42
	300	−76.30	−9.26	13.09	1728	24.58	92.26	50.43	0.89	15.03	144.26	246.00
	350	−70.00	−8.27	16.38	1660	18.09	58.35	54.16	1.39	12.51	112.52	223.65
	400	−68.60	−7.95	14.68	1687	22.34	67.59	64.90	1.20	11.53	117.52	233.35
	450	−65.20	−7.13	15.58	1677	11.39	54.04	61.07	1.25	9.87	138.60	274.27
	500	−65.90	−6.88	15.04	1692	11.81	53.08	61.82	2.67	8.98	153.58	297.18
	550	−60.10	−6.12	17.89	1619	11.86	48.97	50.81	1.59	7.41	97.54	194.86
	600	−62.50	−7.21	15.97	1716	10.64	51.48	51.91	2.40	8.06	188.23	336.36
	650	−63.70	−6.82	15.03	1704	10.83	89.56	48.10	1.69	8.54	142.01	237.13
	700	−67.70	−7.81	17.03	1631	11.71	56.44	45.00	1.24	8.09	108.30	200.42
	750	−69.20	−7.72	15.22	1641	11.02	65.90	44.24	2.39	8.14	109.17	196.32
	800	−69.40	−6.91	15.50	1688	10.26	72.25	42.97	2.26	8.58	151.44	256.75

WC water content by weight, *TDS* total dissolved solids

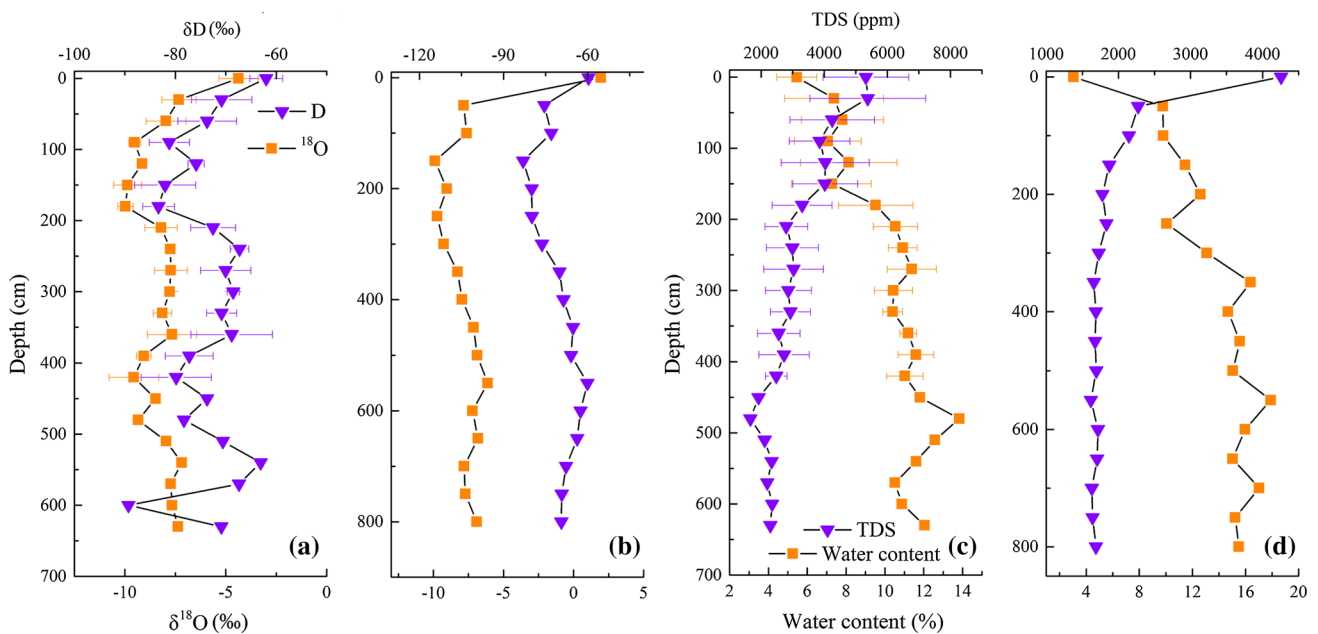**Fig. 7** Variations in $\delta^{18}O$, δD, total dissolved solids (TDS), and water content in soil profiles. **a, b** Share the same legend and label names, and **c, d** share the same legend and label names. **a, c** Show mean ± standard error calculated from soil profiles 1, 2 and 3. **b, d** Show measured value of soil profile 4.

Groundwater demonstrates good mobility, with δD and δ^{18}O values showing possible minor positive drift, but no negative drift. The evaporation line (EL1) was fitted using δD and δ^{18}O values in groundwater, as δD = 4.63δ^{18}O − 30.60 (R^2 = 0.75), and has a smaller slope than those of GMWL and EL2. This suggests that the groundwater is not recharged by local precipitation, but by another source with much depleted isotope characteristics. The δD and δ^{18}O values of reservoirs and rivers surrounding Daihai Lake mostly align along EL1, but not EL2, demonstrating that groundwater is the main water source. Isotope data for Hongshaba Reservoir (R6), and rivers RI2, RI3, and RI5 lie between EL1 and EL2, suggesting that they are sourced from both local precipitation and groundwater, while rivers RI1 and RI4 are mainly recharged by groundwater. The points for Daihai Lake are all located between EL1 and EL2, and much closer to the former, which means that both local precipitation and groundwater recharge the lake, with the latter accounting for a greater proportion.

Soil profiles analysis

All measured data at each depth of the four soil profiles were shown in Table 3. Figure 7a and b show that the δD and δ^{18}O values fall with depth increasing from the surface, then they start to increase at about 200 cm depth, before decreasing again at about 350 cm depth with several fluctuations downward. The δD and δ^{18}O values of the four soil profiles lie far from the EL2 line (Fig. 6), indicating that soil water is not fed by local precipitation. However, most values lie near or significantly overlap those of groundwater, indicating groundwater recharged. The D and ^{18}O contents of precipitation is too low to satisfy the isotopic signatures of soil water; upward percolation of groundwater may be the explanation. The isotopic composition of soil moisture near the surface is much richer than that in deep soil, which can be attributed to intense evaporation. The δD and δ^{18}O profile fluctuations suggest the existence of an evaporation–condensation process during groundwater recharging [36, 37].

It is known that the rainfall can infiltrate unsaturated soil, yet only if sufficient water can accumulate in the soil to meet the maximum field water-holding capacity. During this process, salts within the soil are dissolved and infiltrate downwards with the water. When the infiltration rate slows (or stops), salt transportation ceases and salt accumulation results in a TDS peak. A TDS peak may also occur in the soil surface following intense evaporation and a sustained period of no rainfall. It should be noted that the interaction of groundwater, soil moisture and lake water in the nearshore area may be complex in terms of horizontal and vertical flow. Thus, the high TDS accumulation in the unsaturated zone could be related to zero flux plane (ZFP) behavior, based on total potential.

All the soil profiles have low water contents and high surface TDS, resulting from intense evaporation (Fig. 7c, d). The water content gradually increases with the depth increasing with some fluctuations. The maximum moisture content (13.8%) occurs at 4.8 m. Conversely, the TDS profile of soil water shows a decreasing trend with depth, with a local maximum value at 150 cm depth (Fig. 7c, d), above the depth of the groundwater (not reached in profiles). The TDS value is much higher than that of nearby well water (W14–15 and W30–31; mean TDS = 168 ppm) and spring water (S13; 313 ppm). This suggests that rainfall can only infiltrate to a depth of 150 cm and does not recharge groundwater. PR1 is close to Quanyulin Reservoir (R5) and PR4 is close to Daihai Lake, resulting in stable variations of water content and TDS, and the high TDS accumulation in the profiles may indicate the ZFP. Conversely, PR2 and PR3 are located far from lakes or reservoirs, and the large soil water TDS may be attributed to the effect of groundwater evaporation and condensation [36, 37].

Hydrochemistry analysis

Lithology and soil characteristics can influence the hydrochemistry of infiltrating water; for example, unless mixed with low TDS water or converted to a gas phase, the TDS in a water body increases gradually due to the dissolution of minerals and ions and exchange between rocks and soil [38]. Therefore, the TDS content of a water body can qualitatively reflect flow paths and subsurface water residence times.

Soil water TDS content ranges from 1596 to 8085 ppm, with the highest values near the soil surface, which may result from intense evaporation. The lake water is saline, with TDS content ranging from 5970 to 6580 ppm (L1–L11; Table 1), indicating high evaporation and low precipitation. The TDS content of well, spring, and river water ranges from 112 to 853, 114 to 457, and 415 to 619 ppm, respectively. Despite low precipitation and high surface soil salinity, groundwater and river water remain as good quality fresh waters. The reservoir TDS content ranges from 215 to 3334 ppm (except for R1 and R6), which is consistent with fresh water. Reservoirs R2–4, R8, Quanyulin (R5), and Shimenkou (R7) are re-filled by local people extracting groundwater, resulting in similar TDS values to those of groundwater. In contrast, reservoirs R1 and R6 are recharged by spring fed streams, and the recharge rate is very small relative to the intense evaporation, resulting in high TDS content.

A trilinear Durov diagram highlights distinct differences in TDS values and the chemistry of different water types (Fig. 8). Classified on the basis of TDS, three groups are
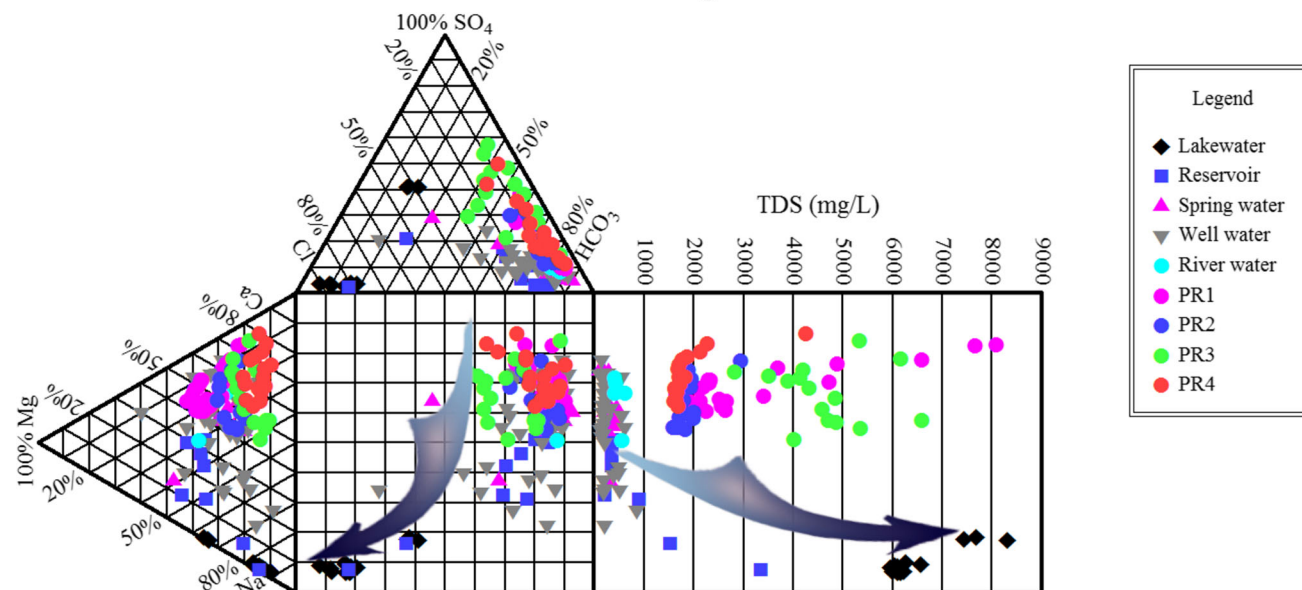
Fig. 8 Durov diagram of different water sources

identified: groundwater and river water are characterized by low TDS; lake water and surface soil water are characterized by high TDS; and deep soil water and reservoir water are characterized by moderate TDS. Considering the impact of evaporation on surface water, this implies that groundwater recharges of rivers and the lake is rapid, but is slowly discharges upwards through the soil.

For Daihai Lake water, the dominant anion is Cl^-, followed by HCO_3^- and SO_4^{2-}, and the dominant cation is Na^+, followed by Mg^{2+} and Ca^{2+}. The chemical compositions of spring, well, soil, and river water are similar, with the dominant cation Ca^{2+}, and the dominant anion HCO_3^-. For reservoir water, the dominant anion and cation are HCO_3^- and Na^+, respectively. Groundwater and river water samples cluster together; and they are tasteless, colorless, and have chemical characteristics of $Ca–HCO_3$ type water, which is common in groundwater systems. Most of the soil water also shows chemical characteristics of $Ca–HCO_3$. In contrast, Daihai Lake water shows chemical characteristics of $Na–Cl$ water types (i.e., saline water). Low Ca^{2+} in Daihai Lake may result from the sedimentation of undissolved $CaCO_3$, as evaporation increases CO_3^{2-}. Variations in the dominant anion and cation also support the discharge of groundwater into the lake and rivers.

Discussion

This study combines isotopes, hydrochemistry, and soil profiles to investigate the water cycle in Daihai Lake basin. The results show that, in additional to local precipitation,

groundwater also supplies water to the lake, and accounts for a greater proportion of recharge. Groundwater also recharges rivers and soil water. Reservoirs seem to be recharged by groundwater, because local people extract groundwater to fill them. However, the groundwater is not fed by local rainfall, but may come from other sources characterized by lower δD and $\delta^{18}O$ values.

If groundwater recharge is of meteoric origin vertically, there are two common recharge mechanisms: preferential flow and the mixture of evaporated soil moisture and subsequent rainfall [39–41]. If groundwater is recharged by precipitation via preferential flow, isotope values should align along EL2, but they actually lie along EL1, which indicates that this assumption is not valid. If groundwater is recharged by precipitation via the mixture of evaporated soil moisture and rain, the isotopic values of soil profiles should decrease with depth to the groundwater level, and groundwater isotope values should be consistent with those of precipitation. However, neither the profiles of isotope and TDS profiles nor the water content support this assumption.

As mentioned above, upward movement of groundwater recharges soil water and rivers. The lake is recharged by local rainfall and groundwater, and evaporation is the only way water consumed. Surface runoff, recharged from local rainfall and groundwater, also supplies water to Daihai Lake. A inferred cross-section of the lake basin demonstrates the pattern of recharge, runoff, and discharge in the region (Fig. 2b). The isotopic evidence implies that groundwater is not recharged from local rainfall but from some other sources characterized by lower δD and $\delta^{18}O$

values. It is consistent with the recent discover of external groundwater recharging in the Hopq Desert (106°52.6′–111°19.2′E, 39°59.2′–40°49.3′N) and Erenhot wasteland (111.4°–113°E, 42.9°–44°N) in Northern China [37, 42], which has been attributed to a fault origin. Therefore, a fault origin for groundwater is inferred in the basin.

Daihai and Huangqihai basin are both rift basins with similar geology and hydrogeology, as well as similar formation and evolution histories. Groundwater from the springs and artesian wells is an important source for both lakes. However, high groundwater consumption has dried the Huangqihai Lake, and in recent years, excessive groundwater use has also triggered significant shrinkage of Daihai Lake. As the groundwater is the largest water source for Daihai Lake, groundwater exploitation should be appropriately limited in the entire basin to avoid the lake drying up.

It is important to note the limitations of the study. Primarily, it is known that single isotopic or hydrochemical comparative analysis is limited, as uncertainty results in multiple potential solutions. Moreover, only four soil profiles were analyzed, which may be not sufficiently representative of soil in the basin. Additionally, the water cycle in the basin is significantly influenced by anthropogenic activities, for example, local people extract groundwater to fill reservoirs. Finally, groundwater recharge cannot be identified by the limited isotopic and hydrochemical data. Therefore, the water cycle inferred here needs to be verified and further investigated, with more detail evidence and additional methods, such as hydrodynamic modeling. Despite these limitations, this study provides valuable information and constraints of isotopes and water chemistry, which will facilitate future research on the water cycle in the basin.

Conclusions

Daihai Lake has faced severe shrinking in recent years, due to excessive use of groundwater. Stable isotopes (D and ^{18}O) and hydrochemistry are used to investigate the Daihai Lake water sources, in order to enable better management. The main conclusions are as follows.

Both local rainfall and groundwater constitute important water sources for the Daihai Lake, but the latter accounts for a slightly great proportion. Groundwater is also an important water source for rivers and soil water. However, groundwater is not recharged from local rainfall, but may come from other sources characterized by lower δD and δ^{18}O values. Combined with springs and artesian wells in the basin, it is consistent with the recent discover of external groundwater recharging in Northern China. As

groundwater contributes the largest water source to the lake, groundwater exploitation should be appropriately limited in the entire basin to avoid the lake drying up.

There are several potential sources of uncertainty in this study, including multiple solutions of isotopic or hydrochemical comparative analysis, the small number of soil profiles, anthropogenic influences, and undetermined source of groundwater recharge. Therefore, further investigation is required in the near future to reduce the uncertainty.

References

1. Chen J, Ji B, Liu Z et al (2013) Isotopic and hydro-chemical evidence on the origin of groundwater through deep-circulation ways in Lake Daihai region, Inner Mongolia plateau. J Lake Sci 25:521–530
2. Zhang J, Lai Z, Jia Y (2012) Luminescence chronology for late Quaternary lake levels of enclosed Huangqihai lake in East Asian monsoon marginal area in northern China. Quat Geochronol 10:123–128
3. Zhang J, Tsukamoto S, Jia Y et al (2016) Lake level reconstruction of Huangqihai Lake in northern China since MIS 3 based on pulsed optically stimulated luminescence dating. J Quat Sci 31(3):225–238
4. Sun Q, Zhou J, Shen J et al (2006) Environmental characteristics of Mid-Holocene recorded by lacustrine sediments from Lake Daihai, north environment sensitive zone, China. Sci China Ser D 49(9):968–981
5. Zhang F, Jin Z, Li F et al (2013) The dominance of loess weathering on water and sediment chemistry within the Daihai Lake catchment, northeastern Chinese Loess Plateau. Appl Geochem 35:51–63
6. Jin Z, Li F, Cao J et al (2006) Geochemistry of Daihai Lake sediments, Inner Mongolia, north China: implications for provenance, sedimentary sorting, and catchment weathering. Geomorphology 80(3):147–163
7. Sun Q, Wang S, Zhou J et al (2009) Lake surface fluctuations since the late glaciation at Lake Daihai, North central China: a direct indicator of hydrological process response to East Asian monsoon climate. Quatern Int 194(1):45–54
8. Xu Q, Li Y, Yang X et al (2005) Source and distribution of pollen in the surface sediment of Daihai Lake, Inner Mongolia. Quat Int 136(1):33–45
9. Wang X, Cui L, Xiao J et al (2013) Stable carbon isotope of black carbon in lake sediments as an indicator of terrestrial environmental changes: an evaluation on paleorecord from Daihai Lake, Inner Mongolia, China. Chem Geol 347:123–134
10. Han Y, Jin Z, Cao J et al (2007) Atmospheric Cu and Pb deposition and transport in lake sediments in a remote mountain area, Northern China. Water Air Soil Pollut 179(1–4):167–181
11. Jiang Z, Liu B, Liu H et al (2014) Trace metals in Daihai Lake sediments, Inner Mongolia, China. Environ Earth sci 71(1):255–266
12. Feng X, Wang Y, Wang Y et al (1994) Survey and assessment of water resources in Daihai Lake Basin with remote sensing information. Hydrology 1994:1–5

13. Carretero SC, Dapeña C, Kruse EE (2013) Hydrogeochemical and isotopic characterisation of groundwater in a sand-dune phreatic aquifer on the northeastern coast of the province of Bbuenos Aires, Argentina. Isot Environ Health Stud 49(3):399–419

14. Murgulet D, Murgulet V, Spalt N et al (2016) Impact of hydrological alterations on river-groundwater exchange and water quality in a semi-arid area: Nueces River, Texas. Sci Total Environ 572(1):595–607

15. Osati K, Koeniger P, Salajegheh A et al (2014) Spatiotemporal patterns of stable isotopes and hydrochemistry in springs and river flow of the upper Karkheh River Basin, Iran. Isot Environ Health Stud 50(2):169–183

16. Wand U, Hermichen WD, Brüggemann E (2011) Stable isotope and hydrogeochemical studies of Beaver Lake and Radok Lake, MacRobertson Land, East Aantarctica. Isot Environ Health Stud 47(4):407–414

17. Liu F, Song X, Yang L et al (2015) Identifying the origin and geochemical evolution of groundwater using hydrochemistry and stable isotopes in the Subei Lake Basin, Ordos energy base, Northwestern China. Hydrol Earth Syst Sci 19(1):551–565

18. Nativ R, Adar E, Dahan O et al (1995) Water recharge and solute transport through the vadose zone of fractured chalk under desert conditions. Water Resour Res 31(2):253–261

19. Koeniger P, Gaj M, Beyer M et al (2016) Review on soil water isotope based groundwater recharge estimations. Hydrol Process 30(16):2817–2834

20. Chen J, Liu X, Wang C et al (2012) Isotopic constraints on the origin of groundwater in the Ordos Basin of northern China. Environ Geol 66(2):505–517

21. Huang T, Pang Z, Edmunds WM (2013) Soil profile evolution following land-use change: implications for groundwater quantity and quality. Hydrol Process 27(8):1238–1252

22. Xiao J, Xu Q, Nakamura T et al (2004) Holocene vegetation variation in the Daihai Lake region of north-central China: a direct indication of the Asian monsoon climatic history. Quat Sci Rev 23(14):1669–1679

23. Hydrological Report (2010) Hydrological data of inland rivers and lakes, Bureau of Hydrology, Ministry of Water Resources, People's Republic of China (**In Chinese**)

24. Epstein S, Mayeda T (1953) Variation of ^{18}O content of waters from natural sources. Geochim Geochim Cosmochim Acta 4(5):213–224

25. Coleman ML, Shepherd TJ, Durban JJ et al (1982) Reduction of water with zinc for hydrogen isotope analysis. Anal Chem 54(6):993–995

26. Hurbaji ARM, Phillips FM, Campbella AR et al (1995) Application of a numerical model for simulating water flow, isotope transport, and heat transfer in the unsaturated zone. J Hydrol 171(1):143–163

27. Liu J, Song X, Sun X et al (2009) Isotopic composition of precipitation over Arid Northwestern China and its implications for the water vapor origin. J Geogr Sci 19(2):164–174

28. IAEA/WMO. Global Network of Isotopes in Precipitation. The GNIP Database. http://www.iaea.org/water. Accessed 1 March 2016

29. Craig H (1961) Isotopic variations in meteoric waters. Science 133(3465):1702–1703

30. Craig H (1961) Standard for reporting concentrations of deuterium and oxygen-18 in natural waters. Science 133(3467):1833–1834

31. Dansgaard W (1964) Stable isotopes in precipitation. Tellus 16(4):436–468

32. Gibson JJ, Edwards TWD, Bursey GG et al (1993) Estimating evaporation using stable isotopes: quantitative results and sensitivity analysis for two catchments in northern Canada. Hydrol Res 24(2–3):79–94

33. Jin K, Rao W, Sun J et al (2015) Isotope characteristics and source of precipitation in the Ordos Desert Area. Yellow River 37(3):31–35 **(In Chinese with English abstract)**

34. Dun Y, Tang C, Shen Y (2014) Identifying interactions between river water and groundwater in the North China Plain using multiple tracers. Environ Earth Sci 72(1):99–110

35. Asano Y, Uchida T, Ohte N (2002) Residence times and flow paths of water in steep unchannelled catchments, Tanakami, Japan. J Hydrol 261(1):173–192

36. Huang D, Chen J, Zhan L et al (2016) Evaporation from sand and loess soils: an experimental approach. Transp Porous Med 113(3):639–651

37. Ge J, Chen J, Ge L et al (2016) Isotopic and hydrochemical evidence of groundwater recharge in the Hopq desert, NW China. J Radioanal Nucl Chem 310(2):1–15

38. Song X, Liu X, Xia J et al (2006) A study of interaction between surface water and groundwater using environmental isotope in Huaisha River basin. Sci China (Ser D) 49(12):1299–1310

39. Yang Y, Shen Z, Weng D et al (2009) Oxygen and hydrogen isotopes of waters in the ordos basin, china: implications for recharge of groundwater in the north of cretaceous groundwater basin. Acta Geol Sin-Engl 83(1):103–113

40. Yin L, Hou G, Su X et al (2011) Isotopes (δD and $\delta^{18}O$) in precipitation, groundwater and surface water in the ordos plateau, china: implications with respect to groundwater recharge and circulation. Hydrogeol J 19(2):429–443

41. Yin L, Hu G, Huang J et al (2011) Groundwater-recharge estimation in the ordos plateau, china: comparison of methods. Hydrogeol J 19(8):1563–1575

42. Zhan L, Chen J, Xu Y et al (2017) Allogenic water recharge of groundwater in the Erenhot wasteland of northern China. J Radioanal Nucl Chem. doi:10.1007/s10967-017-5175-4